

**MOLECULAR DYNAMICS STUDIES
OF THE EFFECTS OF NEURAMINIDASE
MUTATION ON OSELTAMIVIR RESISTANCE**

MUHAMMAD YUSUF

UNIVERSITI SAINS MALAYSIA

2015

**MOLECULAR DYNAMICS STUDIES
OF THE EFFECTS OF NEURAMINIDASE
MUTATION ON OSELTAMIVIR RESISTANCE**

by

MUHAMMAD YUSUF

**Thesis submitted in fulfillment of the requirements
for the Degree of
Doctor of Philosophy**

October 2015

ACKNOWLEDGEMENT

Allah brought you forth from your mothers' wombs, whilst you did not know anything – and gave you hearing and sight and intelligence and affection, for you to be grateful (Holy Qur'an, 16:78). Allah does not burden any human being with a responsibility heavier than he can bear (Holy Qur'an, 2:286)

All praise and gratitude to Allah for His mercy and blessings to me and my family. And thank you to my parents for their unconditional love and constant prayers. I would like to express my most sincere gratitude to my supervisor, Prof. Habibah A. Wahab, for her enormous support and guidance. From her, I have learned a lot. Not only sciences, but also invaluable life-skills and life-lessons; how to endure the shortcomings in phases of life, to have the strength of not giving up, and to believe that in the end there's always a way out. Those are only a few amongst other lessons I have gained under her supervision. I believe that it's Allah's way in answering my prayer to become a better person. To my field supervisor, Prof. Dusanka Janezic, for her endless motivation. To all of my friends in USM, especially in PhDS Lab: Sufian, Imtiaz, Meisam, Azizairol and Dr. Ezatul, Khairi, Hassan, Teh Ban Hong, Faizul, Rina, Dr. Sy Bing, Nadia, Hanim, Adliah, Fatihah, Mazieta, Dya, Shakina, etc. We came from diverse places and cultures, but we've been able to make bonds, strong enough to face hurdle in our life as students: new knowledge to be comprehend, loads of experiments and reports, one-day-assignment, and even personal matters. Special thanks to people amongst my friends: Dr. Belal Omar Mohammad Al-Najjar, Dr. Maywan Hariono and Dr. Muchtaridi who has allowed me to call them brothers. And last but not least, to someone who has made a vow to be my partner in life (and the afterlife inshaAllah) at the first year of my PhD candidature, beloved wife *Andina Septiarani*. Thank you for your unconditional care, support and everything you've given up to let us grow as parents and as an intact family in Penang, far away from our hometown. Special hug and kiss to our 4-years-old little sunshine, *Sakina Alma Sufina*, whose smile and laughter have been the best cure to those long-tiring hectic days. No words can sufficiently describe my gratitude and love for them.

TABLE OF CONTENTS

	Page
ACKNOWLEDGEMENT	ii
TABLE OF CONTENTS	iii
LIST OF TABLES	vii
LIST OF FIGURES	viii
LIST OF ABBREVIATIONS	xvi
ABSTRAK	xviii
ABSTRACT	xx
CHAPTER 1 – INTRODUCTION	1
1.1. Statement of the Problem	1
1.2. Aims and Objectives	4
CHAPTER 2 – LITERATURE REVIEW	5
2.1. Influenza Virus	5
2.2.1. Neuraminidase	14
2.2. The Development of Neuraminidase Inhibitors	17
2.3. Resistance to Neuraminidase Inhibitors	20
2.4. Molecular Dynamics Simulation	28
2.4.1. AMBER Force Field ff03	33
2.4.2. Periodic Boundary Conditions	34
2.4.3. Integration of Motions: Leap-frog Algorithm	36
2.5. Essential Dynamics: Principal Component Analysis	37
2.6. Molecular Docking	39

	Page
2.6.1 Autodock Vina	40
2.6.2 Sliding-box Docking	44
CHAPTER 3 – MATERIALS AND METHODS	48
3.1. Materials	48
3.1.1. Hardware	48
3.1.2. List of Software	48
3.2. Methods	49
3.2.1. Outlines of Research Protocol	49
3.2.2. Preparation of MD System	52
3.2.2(a) WT and H274Y Mutants of N1-subtype	53
3.2.2(b) H274Y Mutant of N2-subtype	53
3.2.2(c) N294S Mutant of N1-subtype	54
3.2.2(d) R292K Mutant of N9-subtype	54
3.2.3 Molecular Dynamics Setup	55
3.2.4. Principal Component Analysis	56
3.2.5. Sliding-box Docking	56
CHAPTER 4 – RESULTS AND DISCUSSION	59
4.1. The Effect of H274Y in N1-subtype	59
4.1.1. The Role of Native-Histidine at Position 274 in WT	59
4.1.2. Conformational Changes in the Vicinity Surrounding Position 274	65
4.1.3 Hydrogen Bond Network in the Vicinity Surrounding Position 274	70
4.1.4 Dihedral Analysis	78

	Page
4.1.5. Essential Dynamics of N1 Binding Site	80
4.1.6. Sliding-Box Docking of OTV and ZMR	84
4.2 The Effect of H274Y in N2-subtype	93
4.2.1. Conformational Changes in the Vicinity Surrounding Position 274 in N2-subtype	95
4.2.2. Hydrogen Bond Network in the Vicinity Surrounding Position 274 of N2-subtype	100
4.2.3. Essential Dynamics of the Binding Site of N2→MT System ...	102
4.2.4. The Role of Residue at Position 245	103
4.2.5. The π -interaction of W295	105
4.3. The Effect of Other Point Mutations in NA	110
4.3.1. The Effect of N294S in N1-subtype	111
4.3.1(a) The Role of Serine at Position 294 in N1-subtype ...	111
4.3.1(b) Effect of N294S Mutation to N1 Binding Site	112
4.3.1(c) Calcium Binding in N294S Mutant	118
4.3.1(d) Hydrogen Bond Network in N294S Binding Site	123
4.3.1(e) Essential Dynamics of N294S System	126
4.3.1(f) Effect of N294S Mutation in N1 on OTV Binding ..	128
4.3.2. The Effect of R292K in N9-subtype	130
4.3.2(a) The Role of Arginine at Position 292 in N9-subtype	130
4.3.2(b) Effect of R292K Mutation to N9 Binding Site	132
4.3.2(c) Hydrogen Bond Network in R292K Mutant	138
4.3.2(d) Essential Dynamics of N9 Subtype due to R292K Mutation	140
4.3.2(e) Effect of R292K Mutation in N9 on OTV Binding ..	141
4.4 Further Discussion	143

	Page
CHAPTER 5 – CONCLUSION	154
5.1. Accomplishment of Research Objectives	154
5.2. Future Work	157
5.3. Concluding Remark	158
REFERENCES	160
APPENDICES	172
Appendix 1: Salt Concentration in MD Simulation	
Appendix 2: Comparative Modeling of N9→WT System	
Appendix 3: Examples of Input and Output Files of AMBER	
Appendix 4: Positive Control Docking and Sliding-Box Docking Results for Each Snapshot	
Appendix 5: Complete H-bond Analysis in WT, MT, YH→MT, and HY→WT systems throughout 20 ns of MD simulation.	
Appendix 6: Pairwise Decomposition of the Interaction Energies between Two Residues	
Appendix 7: Timeline Mechanism of N1’s Binding Site Disruption due to H274Y	
LIST OF PUBLICATION	

LIST OF TABLES

	Page
Table 2.1. The effect of different size of amino acid's side chain at the position of 274 towards Km values of 2'-(4-Methylumbelliferyl)- α -D-N-acetylneuraminic acid (MUNANA) and Ki values of OTV, ZMR, and 4-amino-DANA (adapted from Wang et al., 2002).	22
Table 2.2. Average buried surface area (BSA) of atoms involved in interaction between NA's active site and OTV's pentyloxy group resulted from WT, H274Y, N294S, and Y252H (Ripoll et al., 2012).	26
Table 2.3. Activity, binding and kinetic parameters of OTV and ZMR towards N1 neuraminidase (Collins et al., 2008).	28
Table 2.4. Scoring function weights and terms in AutoDock Vina (Trott and Olson, 2010).	43
Table 3.1. The list of MD systems to elucidate the mechanism of H274Y, N294S, and R292K in apo state of NA.	52
Table 4.1. Time evolution of hydrogen bond formation among residues within 5 Å from position 274 in WT, MT, YH→MT, and HY→WT systems throughout 20 ns of MD simulation, which shows notable differences between WT and H274Y systems.	72
Table 4.2. List of OTV derivatives that docked to the entrance of Path-1. ...	90
Table 4.3. Time-evolution plot of H-bond formation in N2→MT system throughout 20 ns of MD simulation.	101
Table 4.4. Pairwise decomposition of the interaction energies between two residues.	102
Table 4.5. Time evolution plot of H-bond formation in N1→NS systems throughout 20 ns of MD simulations.	123
Table 4.6. Time evolution plot of H-bond formation amongst E276, R292, and N/S294 in N1→WT, N1→HY, and N1→NS systems throughout 20 ns of MD simulations.	125
Table 4.7. Hydrogen bond analysis of N9→WT and N9→RK systems.	139

LIST OF FIGURES

	Page
Figure 2.1. Four drug target of influenza virus: HA, NA, M2 ion channel and ribonucleoprotein (RNP) (taken from http://www.cdc.gov/flu/images/h1n1/3D_Influenza_transparent_key_pieslice_lrg.gif).	6
Figure 2.2. Life cycle of influenza A virus (Das et al., 2010).	8
Figure 2.3. Antigenic shift in influenza virus. (US National Institute of Allergy and Infectious Diseases (NIAID)).	10
Figure 2.4. Antigenic drift in influenza virus (US National Institute of Allergy and Infectious Diseases (NIAID)).	12
Figure 2.5. Genetic relationship of influenza virus among human, swine, and avian influenza A gene pool (taken from Morens et al., 2009).	12
Figure 2.6. (a) Homotetramer NA which binding site located on top region. NA binding site composed mostly by polar residues (adapted from Stoll et al., 2003). (b) Residues within 5 Å from OTV in N1- and N2- subtypes (colored in green and orange, respectively). The figure was generated using Accelrys Visualizer and VMD.	16
Figure 2.7. Three dimension chemical structures of NANA (substrate), DANA, ZMR, OTV, PMV, LNV and LNV octanoate. The figure was generated using Accelrys Visualizer.	20
Figure 2.8. Binding mode interaction of OTV (green colored sticks) in NA's active site and the overview of hypotheses on H274Y effects towards the mechanism of OTV resistance. The figure was generated using Accelrys Visualizer.	21
Figure 2.9. (a) The molecular basis of N1 resistance towards OTV derived from H274Y crystal structure (PDB ID 3CL0, green colored carbon atoms) which overlaid with wild type (yellow colored carbon atoms). (b) The overlaid of H274Y-ZMR complex (PDB ID 3CKZ, green colored carbon atoms) with wild type (Collins et al., 2008).	23
Figure 2.10. Rotational changes of binding residues (Y274, E276 and R224) and pentyloxy group of OTV (Tor-X, Tor-Y and Tor Z) which represented in (a) molecular diagram and (b) plot of dihedral angle distribution (taken from Malaisree et al., 2009).	24

Figure 2.11.	(A) The interaction between OTV and NA wild type. (B) Water infiltration into the binding site of pentyloxy group of OTV reduce the hydrophobic packing between the drug and receptor (Park and Jo, 2009).	25
Figure 2.12.	The representative structures of (A) ZMR-WT, (B) ZMR-H274Y, (C) ZMR-N294S, (D) OTV-WT, (E) OTV-H274Y, and (F) OTV-N294S from Hamiltonian Replica Exchange MD simulations (Ripoll et al., 2012). Hydrogen bond is represented by dashed red line.	25
Figure 2.13.	The unbinding and binding pathway of OTV through negatively charged (red colored molecular surfaces) electrostatic binding funnel resulted from 100 ns of MD simulations (Le et al., 2010).	27
Figure 2.14.	Computer simulations as a bridge between theory and experiment (Attig et al., 2004).	29
Figure 2.15.	General flow chart of MD simulations in present work.	33
Figure 2.16.	Periodic boundary conditions on two dimensions. r_{cut} is the cutoff radius. (http://www.compsoc.man.ac.uk/~lucky/Democritus/Pictures/psc-mi.gif) [Accessed 1/7/2014].	35
Figure 2.17.	Comparing the scoring function and search algorithm of AutoDock 4 and Vina (Chang et al., 2010).	41
Figure 2.18.	Weighted scoring function term combinations in AutoDock Vina (Trott and Olson, 2010).	43
Figure 2.19.	Scheme of sliding-box docking using multiple binding box to find the best complementarity between ligand and particular DNA sequence (Martins-José, 2013).	45
Figure 2.20.	The resulted docking conformations of OTV on neuraminidase H5N1 which represented by their centroids (Tran et al., 2013). ...	46
Figure 2.21.	Two possible binding pathways of oseltamivir into neuraminidase H5N1 active site (Tran et al., 2013).	46
Figure 3.1.	Outlines of research protocol.	50
Figure 3.2.	General workflow of MD simulation.	51
Figure 3.3.	The placement of grid boxes (searching space) which started from the top surface of NA to the active site. Active site residues are displayed in sticks representation. The figure was generated using AutoDockTools.	57

	Page
Figure 4.1. Four possible interactions of H274 with neighboring residues from 250-loop and 300-loop (visualized in green colored lines) based on the crystal structure PDB ID 2HU4 (Russell et al., 2006).	59
Figure 4.2. Time evolution plot of RMSD protein backbone throughout 20 ns of MD simulation. The bold lines are moving averages over 100 data points. The figure was generated using MS Excel.	60
Figure 4.3. The RMSF of backbone for each residue of NA throughout 20 ns of MD simulation. The marked differences in RMSF are highlighted using boxes. The figure was generated using MS Excel.	61
Figure 4.4. The average structures of (a) HID, (b) HIE, (c) HIP, and (d) MT systems and the time evolution snapshots of (e) HID, (f) HIE, (g) HIP, and (h) MT, captured every 2 ns, from 20 ns of simulations. Hydrogen bond and salt bridge are depicted in green dashes and yellow lines, respectively. Figures (a-d) and (e-h) were generated using Accelrys Visualizer and VMD, respectively.	62
Figure 4.5. The time evolution RMSD of NA's backbone in four studied systems: WT, MT, YH→MT, and HY→WT. The bold lines are moving averages over 100 data points. The figure was generated using MS Excel.	66
Figure 4.6. RMSF values of protein backbone in WT (green), YH→MT (red), MT (orange), and HY→WT (blue) systems. Loops around position 274, i.e. 250-, 270-, 300- and 340-loops, are highlighted by box. The figure was generated using MS Excel and Accelrys Visualizer.	67
Figure 4.7. The superimposed conformations of (a) WT, (b) YH→MT, (c) MT, and (d) HY→WT extracted from 2-20 ns at interval 2 ns. The time evolution snapshots is reflected by gradient red-white-blue colors. The figure was generate using VMD.	69
Figure 4.8. (a) The architecture of NA binding site, (b) Amino acid residues of NA binding site within 5 Å from position 274. Members of 270-loop are colored in red. Those residues from 250-loop and 300-loop directions are colored in orange and purple, respectively. Figures (a) and (b) were generated using VMD and Accelrys Visualizer, respectively.	71
Figure 4.9. Illustration of OTV binding with (a) WT and (b) final snapshot of MT system (H-bond of E276-R292 formed polar environment at hydrophobic sub-pocket for OTV). The figure was generated using Accelrys Visualizer.	76

Figure 4.10	Pairwise decomposition of the interaction energies between two residues. The figure was generated using MS Excel.	77
Figure 4.11.	Dihedral angle plot of (a) H296, (b) W295, and (c) H/Y274 over 20 ns of simulation. The time evolution conformational changes of these residues and loops in (d) YH→MT and (e) MT systems are presented using gradient color red-white-blue. Figures (a-c) and (d-e) were generated using MS Excel and VMD, respectively.	79
Figure 4.12.	Essential dynamics of (A) WT, (B) MT, (C) YH→MT, and (D) HY→WT systems. Area inside dashed-box covers the loops around position 274. The arrows represented the amplitude and direction of movement. The figure was generated using VMD. ...	81
Figure 4.13.	The superimposed conformations of WT (transparent green) and MT (orange) which taken from MD trajectories at 20 ns. Green, maroon, and white dashed lines are H-bond, amide- π stacked, and π -donor H-bond interactions, respectively. The figure was generated using Accelrys Visualizer.	82
Figure 4.14.	Plot of sliding-docking results: (a) OTV and (b) ZMR on WT system at 0 ns; (c) OTV and (d) ZMR on WT system at 20 ns; (e) OTV and (f) ZMR on MT system at 20 ns. Boxes presented the empty binding site surface which are composed of 150-, 250-, 270-, 300-, and 340- loops. Binding pathways are proposed by the gradient color of ligands: red to orange to green colors. The figure was generated using Accelrys Visualizer.	85
Figure 4.15.	Plot of OTV's centroids on (a) WT system at 0 ns (<i>left</i>) and (b) MT at 20 ns (<i>left</i>); ZMR's centroids on (b) MT at 20 ns (<i>right</i>). Energy profile of OTV binding into WT at 0 ns shown in (a) (<i>right</i>). Grey colored bars indicated the range docking score of ligands. Average of each bar indicated with black line which provided with its standard error of mean (smaller black line). The figure was generated using Accelrys Visualizer.	87
Figure 4.16.	The role of ZMR' glycerol moiety in the interaction with R371 to reach the active site through 340-loop in MT system. The figure was generated using Accelrys Visualizer.	88
Figure 4.17.	Predicted binding pathway of PMV to the MT system at 20 ns. Similar hydrophobic group in OTV and PMV are highlighted by dotted circles. The figure was generated using Accelrys Visualizer.	89

Figure 4.18.	Docking pose(s) of OTV derivatives that form H-bond with the exposed-R371 in MT snapshot at 20 ns. H-bond is represented by green dashed-line. The figure was generated using Accelrys Visualizer.	91
Figure 4.19.	End-point interaction of (a) OTV and (b) ZMR with the last snapshot of MT system at 20 ns. Hydrogen bond and salt bridge represented by green and yellow dashed lines, respectively. Docked poses of OTV and ZMR visualized in green colored sticks, whereas co-crystal structure of OTV visualized by grey color. The figure was generated using Accelrys Visualizer.	93
Figure 4.20.	The overlaid structures of N1 and N9 subtypes. At position 252, N1 has tyrosine while N9 has threonine (Russell et al., 2006).	94
Figure 4.21.	Residual RMS fluctuation of protein backbone of N2→MT (black line); WT and MT of N1-subtype (green and red line, respectively), throughout 20 ns of simulation. The figure was generated using MS Excel.	97
Figure 4.22.	The superimposed conformations of (a) N2→MT, (b) WT(N1) and (c) MT(N1) systems that extracted from 2-20 ns at interval of 2. The time evolution snapshots is reflected by gradient red-white-blue colors. The figure was generated using VMD.	99
Figure 4.23.	Overlaid structures of the final snapshot of (a) N2→MT (grey color) and (b) WT(N1) (orange color) with that of WT(N1) (transparent green color). Green, maroon, and white dashed lines are H-bond, amide- π stacked, and π -donor H-bond interactions, respectively. The figure was generated using Accelrys Visualizer.	100
Figure 4.24.	Essential dynamics of N2→MT compared with WT and MT of N1-subtype. The arrows represented the magnitude and direction of motions. The figure was generated using VMD.	103
Figure 4.25.	The different residue at position 245 in (a) PDB 1NN2 and (b) PDB 2HTY. (c) Sequence alignment of between 250-loop in N1 (PDB 2HTY) and N2-subtype (PDB 1NN2). 250-loop is highlighted with red box. The figure was generated using Accelrys Visualizer.	104
Figure 4.26.	Stacking pattern of (a) K296-W295-R249 in N2-subtype, and (b) H296-W295-Q249 in N1-subtype (PDB 1NN2 and 2HTY, respectively). The figure was generated using Accelrys Visualizer.	106

	Page
Figure 4.27. The time evolution changes of stacking pattern (a) K296-W295-R249 in N2→MT and (b) H296-W295-Q249 in MT(N1) throughout 20 ns of MD simulations. The figure was generated using Accelrys Visualizer.	108
Figure 4.28. (a) Stacking pattern among residues 296-295-249 in N1- and N2-subtypes. Pair of atoms used to monitor the distance among three residues are highlighted in red colored text and lines. The plot of distances between (b) residues 259 and 296; and (c) between residues 295 and 249 throughout 20 ns of simulations. Figures (a) and (b-c) were generated using Accelrys Visualizer and MS Excel, respectively.	109
Figure 4.29. Role of N294 in NA binding site (PDB ID 2HU4). H-bond, π - π , and π -cation are depicted in green, pink, and maroon colored dashed lines. The figure was generated using Accelrys Visualizer.	111
Figure 4.30. The intermolecular interaction network of N294 which taken from the 20 ns-average structure of WT(N1) system (sub-chapter 4.1). The unit of distance is angstrom. The figure was generated using Accelrys Visualizer.	112
Figure 4.31. The time evolution RMSD of NA's backbone in N1→NS compared to N1→WT and N1→HY systems. The bold lines are moving average of each 100 data. The figure was generated using MS Excel.	113
Figure 4.32. RMSF values of N1's backbone in WT (green color), N1→HY (red color), and N1→NS (purple color) systems. Loops around position 274 with marked differences of fluctuations are highlighted inside box. Inset is the top overview of N1 binding site in complex with OTV (PDB ID 2HU4). The figure was generated using Accelrys Visualizer and MS Excel.	116
Figure 4.33. The superimposed conformations of (a) N1→NS, (b) N1→WT, and (c) N1→HY extracted from 2-20 ns at interval 2. The time evolution snapshots is reflected by gradient red-white-blue colors. The figure was generated using VMD.	117
Figure 4.34. Time evolution snapshots of 340-loop and surrounding region in N1→NS system from 20 ns of MD simulation. The figure was generated using VMD.	118
Figure 4.35. The calcium binding site at NA (based on PDB ID 2HTY). The unit of distance is in angstrom. The figure was generated using Accelrys Visualizer.	118

	Page
Figure 4.36. The overlaid averaged structures of N1→NS (grey color) and N1→WT (blue color) systems. The figure was generated using Accelrys Visualizer.	120
Figure 4.37. The overlaid averaged structures of N1→NS (grey color) and N1→HY (orange color) systems. The figure was generated using Accelrys Visualizer.	120
Figure 4.38. Time-evolution plot of distances between a conserved calcium ion and its surrounding atoms in (a) N1→WT, (b) N1→HY, and (c) N1→NS. The figure was generated using MS Excel.	122
Figure 4.39. Essential dynamics of protein backbone of (a) N1→WT, (b) N1→HY, and (c) N1→NS systems throughout 20 ns of simulation. The figure was generated using VMD.	127
Figure 4.40. Sliding-box docking results of OTV on the final snapshot of N1→NS system. Residues behind the molecular surface of 250-loop surface are shown in the inset. The figure was generated using Accelrys Visualizer.	129
Figure 4.41. The role of R292, as part of triad arginine (highlighted by green color), in stabilizing carboxyl group of the ligand. PDB ID 1F8B (Smith et al., 2001). The figure was generated using Accelrys Visualizer.	130
Figure 4.42. Interaction between OTV and (a) WT and (b) R292K mutant of N9-subtype (Woods et al., 2013b).	132
Figure 4.43. Time evolution plot of RMSD values in N9→WT, N9→RK, N1→WT, and N2→MT throughout 20 ns of simulation.	133
Figure 4.44. RMSF plot of N9→WT and N9→RK in comparison with N2→MT system. Residues 283-287 and 354-358 which located at the bottom of 300-loop and 340-loop, are highlighted in the inset picture.	134
Figure 4.45. The superimposed conformations of (a) N9→WT and (b) N9→RK systems which extracted from 2-20 ns at interval 2. The time evolution snapshots is reflected by gradient red-white-blue colors. The figure was generated using VMD.	136
Figure 4.46. Time evolution snapshots of stacking pattern Q296-W295-P249 in (a) N9→WT and (b) N9→RK systems throughout 20 ns. The figure was generated using VMD.	136

	Page
Figure 4.47. The average structures of N9→WT and N9→RK systems. The inset showed the close-up interactions between residue 292 and E277. The figure was generated using Accelrys Visualizer.	137
Figure 4.48. Essential dynamics of (a) N9→WT and (b) N9→RK systems throughout 20 ns. The figure was generated using VMD.	141
Figure 4.49. Sliding-box docking result of OTV on the last snapshot of N9→RK system. The figure was generated using Accelrys Visualizer.	142
Figure 4.50. (a) Atypical peptide bond between S342-S344 in PDB ID 3CKZ. Positive contour of electron density maps of crystal structure of H274Y in complex with (b) ZMR (3CKZ) and (c) OTV (3CLO). (d) Fully resolved peptide bond of S342-S344 in crystal structure of WT (2HTY). Figures a and b-d were generated using Accelrys Visualizer and WinCoot, respectively.	146
Figure 4.51. Proposed mechanism of binding site disruption in H274Y system. The figure was generated using Accelrys Visualizer.	148
Figure 4.52. (a) The conformation of 340-loop in MT at 20 ns (dark-blue color), YH→MT at 20 ns (orange color) and at 40 ns (light-blue color). Conformation of W295 and 340-loop in (b) PDB 3CKZ, (c) MT at 20 ns, (c) YH→MT at 20 ns, and (d) YH→MT at 40 ns. The distance between W295 and G345 in YH→MT was monitored from 20 - 40 ns. Figures a-e and f were generated using Accelrys Visualizer and MS Excel, respectively.	149

LIST OF ABBREVIATIONS

A (ALA)	Alanine
AMBER	Assisted Model Building with Energy Refinement
AUC	Area Under the Curve
C (CYS)	Cysteine
CDC	Centers for Disease Control and Prevention
CPU	Central Processing Unit
D (ASP)	Aspartic Acid
DANA	2,3-didehydro-2-deoxy-N-acetylneuraminic acid
DNA	Deoxyribonucleic acid
DUD	Database Useful for Decoy
E (GLU)	Glutamic Acid
EDA	Essential Dynamics Analysis
F (PHE)	Phenylalanine
FDA	Food and Drug Administration
FF	Force Field
G (GLY)	Glycine
GA	Genetic Algorithm
GPU	Graphics Processing Unit
H (HIS)	Histidine
HA	Hemagglutinin
H-bond	Hydrogen Bond
HID	Histidine with delta nitrogen protonated
HIE	Histidine with epsilon nitrogen protonated
HIP	Histidine with both nitrogens protonated
HY	Mutation from histidine to tyrosine
I (ILE)	Isoleucine
ILS	Iterative Local Searching
K (LYS)	Lysine
L (LEU)	Leucine
LAN	Local Area Network
LNV	Laninamivir
M (MET)	Methionine
MD	Molecular Dynamics
MM/GBSA	Molecular Mechanics/Generalized Born Surface Area
MM/PBSA	Molecular Mechanics/Poisson Boltzmann Surface Area
MT	Mutant type
MUNANA	2'-(4-Methylumbelliferyl)- α -D-N-acetylneuraminic acid
N (ASN)	Asparagine
NA	Neuraminidase
NANA	N-acetylneuraminic acid
NPT	Constant number of particle (N), pressure (P) and temperature (T)
ns	Nanosecond
NS	Mutation from asparagine to serine
NVT	Constant number of particle (N), volume (V) and temperature (T)
OTV	Oseltamivir
P (PRO)	Proline

PBC	Periodic Boundary Conditions
PCA	Principal Component Analysis
PDB	Protein Data Bank
PME	Particle Mesh Ewald
PMV	Peramivir
Q (GLN)	Glutamine
R (ARG)	Arginine
RAM	Random-access Memory
RFU	Relative Fluorescence Unit
RK	Mutation from arginine to lysine
RMSD	Root Mean Square Deviation
RMSF	Root Mean Square Fluctuation
RNA	Ribonucleic Acid
RNP	Ribonucleoprotein
S (SER)	Serine
T (THR)	Threonine
V (VAL)	Valine
VMD	Visual Molecular Dynamics
W (TRP)	Tryptophan
WT	Wild type
Y (TYR)	Tyrosine
ZMR	Zanamivir

KAJIAN DINAMIK MOLEKUL
KESAN MUTASI NEURAMINIDASE
KEPADA RINTANGAN OSELTAMIVIR

ABSTRAK

Peningkatan laporan mengenai virus influenza yang resistan terhadap oseltamivir (OTV) (contohnya mutasi H274Y pada neuraminidase, NA) telah menarik banyak perhatian para penyelidik. Banyak kajian telah dilakukan untuk memahami mekanisme rintangan OTV pada NA H274Y. Namun, sebahagian besar kajian pada H274Y hanya tertumpu kepada sistem ubat-terikat, sementara kesan langsung mutasi terhadap NA sendiri, sebelum mengikat ubat, masih belum jelas. Oleh itu, analisis dinamik molekul NA pada bentuk apo, diikuti dengan analisis komponen utama dan pengiraan tenaga interaksi, telah dijalankan untuk mengkaji perubahan struktur pada tapak ikatan NA, sebagai kesan daripada mutasi H274Y. Gangguan tapak ikatan NA kerana mutasi H274Y bermula daripada kesan tolakan Y274 pada loop-250 telah menyebabkan perubahan jaringan ikatan hidrogen di sekitar residu 274. Putaran rantai sisi W295 telah menyebabkan loop-340 bergerak ke atas dan mengakibatkan laluan pengikatan OTV telah terjejas kerana gangguan dari tapak ikatan NA, berdasarkan laporan sliding-box docking. Kajian ini juga memperlihatkan pentingnya kelompok berfungsi pada kedudukan C6 dari asid sialik. Selain itu, dua hal yang mungkin boleh digunakan untuk menjelaskan perbezaan kesan H274Y pada subjenis N1 dan N2 ialah: residu 245 dan residu yang membentuk interaksi π dengan W296. Pendekatan yang sama telah dilakukan untuk menjelaskan kesan mutasi N294S subjenis N1 dan R292K subjenis N9. Gangguan pengikatan kalsium terjadi pada mutan N294S, dan perubahan

struktur teras NA telah berlaku pada mutan R292K. Buat pertama kalinya, mekanisme rintangan OTV telah dikaji secara terperinci dalam situasi sebelum NA sebelum terikat ubat. Hasil kajian ini diharapkan dapat meningkatkan kefahaman mengenai kes rintangan OTV dan bermanfaat untuk reka bentuk ubat anti influenza yang baru.

MOLECULAR DYNAMICS STUDIES
OF THE EFFECT OF NEURAMINIDASE MUTATION
ON OSELTAMIVIR RESISTANCE

ABSTRACT

The increased number of reports on oseltamivir (OTV) resistant strains of influenza virus (e.g. H274Y mutation on its neuraminidase, NA) has created some causes for concern. Many studies have been conducted to uncover the mechanism of OTV resistances in H274Y NA. However, most of the reported studies on H274Y were only focused on drug-bound-system, while direct effects of the mutation towards NA itself, prior to drug binding, remains unclear. Therefore, molecular dynamics of NA in apo-form, followed by principal component analysis and interaction energy calculation, were performed to investigate the structural changes of NA binding site, as a result of H274Y mutation. The disruption of NA binding site due to H274Y, initiated by the repulsive effect of Y274 on 250-loop - which in turn altered the hydrogen bond network around residue 274, was observed. The rotated W295 side chain has caused the upwards movement of 340-loop. Consequently, sliding-box docking results suggested that the binding pathway of OTV was compromised due to this binding site disruption. This study also highlighted the importance of functional group at position C6 of sialic acid mimicry. Moreover, two possible keys to explain the differences of H274Y effects in N1- and N2- subtypes, were proposed: residue 245, and the residue which formed π -interaction with W296. Similar approaches were applied to explain the effects of N294S and R292K mutations in N1- and N9- subtypes, respectively. The disruption of calcium binding in N294S mutant was observed. While

the changes of NA's core structure occurred in R292K mutant. For the first time, the mechanism of OTV resistance was extensively studied from the state of NA prior to drug binding. It is hoped that these results could improve the understanding of OTV resistances and shed some light on the design of novel anti-influenza drug.

CHAPTER I

INTRODUCTION

1.1. Statement of the Problem

Influenza, also referred to as “flu”, is a disease which transmission could reach pandemic levels. The worst influenza pandemic was estimated to have killed more than 50 million people in year 1918 (Taubenberger and Morens, 2006). Influenza is caused by influenza virus, which has evolved and mutated over time, posing serious challenges in developing effective therapies. In the last century, at least three influenza pandemics have been reported: Spanish Flu (H1N1) in year 1918, Asian Flu (H2N2) in year 1957 and Hongkong Flu (H3N2) in year 1968. In 2009, a pandemic swine flu (H1N1) which has killed about 18,500 people, was reported. To complicate matters, avian influenza virus, that originally carried among birds (e.g. H5N1), has also been a major threat due to its high fatality rate when transmitted to human. In 2011, 34 deaths out of 62 cases of H5N1 were reported from Bangladesh, Cambodia, China, Egypt, and Indonesia (Health & Human Services, 2013). In 2013, a novel avian influenza virus, H7N9, which was not previously known to infect human, has resulted in 37 deaths out of 132 patients in China (CDC, 2013; WHO, 2013a; WHO, 2013b).

The glycoproteins on the surface of influenza virus, i.e. hemagglutinin (HA) and neuraminidase (NA), have become the targets for the development of anti-influenza (as reviewed in Itzstein and Thomson, 2009). Up to 2013, there have been

18 HA and 11 NA subtypes of influenza (Tong et al., 2013). Although HA is the main target for vaccine development, to develop ligands that can tightly bind to HA is very challenging. It is due to the shallow and less-energetic receptor binding site of HA (Yusuf et al., 2013). Whilst structural conservation of NA binding site, NA's important role in viral infection, and the availability of NA crystal structures in Protein Data Bank are the major reasons NA is the most targeted protein for inhibitors in anti-influenza drug design (as reviewed in Itzstein and Thomson, 2009). Tamiflu (a prodrug for oseltamivir carboxylate, OTV) and Relenza (zanamivir, ZMR) are two examples of NA inhibitors approved by FDA to be released to the market.

Although Tamiflu is the world's largest stockpile of anti-influenza drug, and most dominantly used for influenza treatment, the increased report of OTV resistant strains (e.g. H274Y, R292K, N294S, including the recent H7N9 China strain) has created some causes for concern (Moscona, 2005; Hayden, 2006; Abed et al., 2006, Hurt et al., 2009; Soundararajan et al., 2009; Liu et al., 2013; Gillman, 2015). Hurt et al. (2009) reported that 64% of H1N1 samples from ten countries including Australia, Malaysia, and South Africa were of H274Y mutants. Moreover, 70% occupancy of H274Y in H1N1, circulating in Norway, has indicated that the mutant is transmissible among humans, even in the absence of drug pressure (Stephenson et al., 2009). Recently, an *in vitro* study showed that once the virus evolved, H274Y mutation persisted after the withdrawal of the drug in the experiment (Renzette et al., 2014). All these phenomena suggest the careful use of OTV to limit the development of mutant virus. It is noted that the efficacy of ZMR to H1N1 was not affected by H274Y mutation. However, ZMR showed poor oral bioavailability due to its polarity problem.

Therefore, deep understanding on the mechanism of OTV resistances, especially at the molecular/atomic level, has become very important. To date, there are many studies on mutagenesis (Wang et al., 2002), crystallography (Collins et al., 2008), and molecular dynamics simulation (Malaisree et al., 2009; Park and Jo, 2009; Wang and Zheng, 2009; Le et al., 2010; Rungrotmongkol et al., 2010; Karthick et al., 2012) have been conducted in the attempts to uncover the mechanism of OTV resistances in NA. However, most of reported studies on OTV resistances were focused on the changes of drug-receptor interaction of OTV (Malaisree et al., 2009; Park and Jo, 2009; Wang and Zheng, 2009; Rungrotmongkol et al., 2010; Li et al., 2012; Ripoll et al., 2012; Woods et al., 2012; Woods et al., 2013), while the direct consequence of these mutation points towards the dynamics behavior of NA binding site, albeit prior to drug binding, still remains unclear. Molecular dynamics (MD) simulation has been a valuable method to investigate the structural behavior of protein, and also to rationally predict the “future state” of a particular conformation. Hence observing the mutation effect to NA’ structure has become feasible through MD simulation. A mutagenesis study by Wang and colleagues (Wang et al., 2002) implied that the native-histidine itself, at position 274, might have a distinct role in the wild type NA. Understanding of the role of H274 should be useful to interpret the structural changes of NA binding site that occurred due to mutation, when histidine being replaced with tyrosine (H274Y). It is worth noting that histidine has three possibilities of protonation states in physiological pH. Moreover, the affinity of OTV towards H274Y-carrying N2-subtype was unaffected, indicating the importance of residues surrounding the mutation point. In addition, N294S and R292K, respectively N1 and N9 subtypes, are the other mutations which

related to OTV resistances. The effect of these two mutations to the structural behavior of NA, prior to drug binding, is also still elusive.

1.2. Aims and Objectives

Based on the problem statement above, the aim of this work is to study the mechanism of OTV resistances in NA using molecular dynamics simulations of various NA systems in apo (ligand-free) form. Specifically, the objectives of this work were to investigate:

1. the specific role of native-histidine at position 274 in wild type,
2. the direct effects of H274Y to the integrity of NA binding site,
3. the effects of H274Y in relation with OTV binding,
4. the effects of H274Y in N2-subtype, and to compare with that in N1-subtype,
5. the effects of N294S and R292K mutations on N1 and N9 subtypes, respectively.

CHAPTER II

LITERATURE REVIEW

2.1. Influenza Virus

Influenza virus is an RNA virus of Orthomyxoviridae family, which serologically divided into three subtypes: A, B, and C. Influenza A virus possesses higher pathogenicity to human compared to Influenza B and C. Influenza A has 8 RNA segments, i.e. NA, HA, NP, NS, M2/M1, PA, PB1 and PB2. Amongst these, four gene products have been targeted for drug development, i.e. HA, NA, M2 and RNP (Figure 2.1) (Du et al., 2012; CDC, 2009). RNP (ribonucleoprotein) is formed by NP, RNA, and three polymerase subunits (PA, PB1 and PB2) (Du et al., 2012).

Influenza virus A is named based on the subtypes of its two main surface glycoproteins: hemagglutinin (HA) and neuraminidase (NA) (as reviewed in Itzstein and Thomson, 2009). There are 18 and 11 subtypes of HA and NA, respectively (Tong et al., 2013).

HA, a surface glycoprotein of influenza virus (Skehel and Wiley, 2000) plays a role in receptor-binding (sialic acid) and membrane fusion glycoprotein of the influenza virus (Wiley and Skehel, 1987). Due to its high immunogenicity, HA is a main target for vaccine development although development of small-molecule inhibitors of HA has also been reported (Matsubara et al., 2010; Gambaryan et al., 2008). The major challenge in targeting HA for vaccine is the accumulated mutations

in its antigenic site. In addition, its shallow and less-energetic binding site also contributed to the challenge in developing ligand which can tightly bind on HA (Yusuf et al., 2013).

NA is another glycoprotein on the surface of influenza virus, which function is to remove terminal sialic acid from mucins thus helps HA to disaggregate, which in turn allows the virus to finally reached the host cell (Wagner et al., 2002). NA is also required at the last stage of infection by removing NANA (neuraminic/sialic acid) from the viral envelope thus releasing the virus progeny to further infect another host cell (Palese et al., 1974).

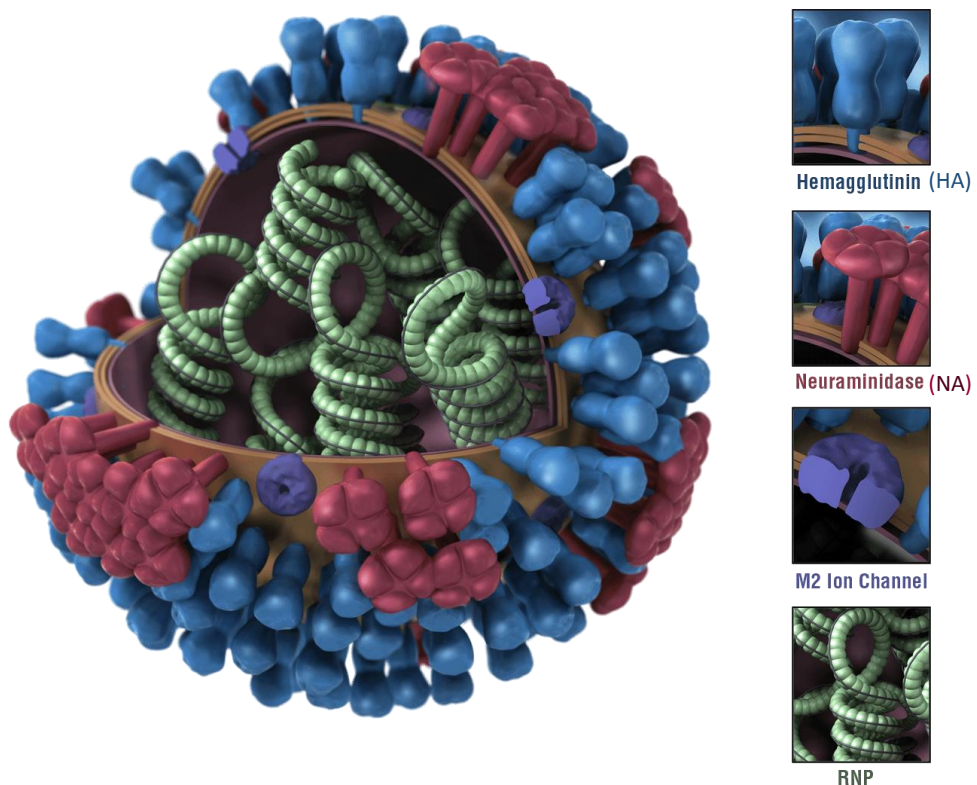


Figure 2.1. Four drug target of influenza virus: HA, NA, M2 ion channel and ribonucleoprotein (RNP) (taken from http://www.cdc.gov/flu/images/h1n1/3D_Influenza_transparent_key_pieslice_lrg.gif).

A comprehensive life cycle of influenza A virus is presented in Figure 2.2 (Das et al., 2010). In order to enter the virus cell, initially, HA binds to the sialic acid receptor on the surface of host cell. Low pH in endosome, which is supposed to be the defense mechanism of cell against foreign material, triggers a conformational change in HA which allows the virus fusion with endosomal membrane (endocytosis). In addition, the acidic condition also enables protons to flow into the virus through M2 ion channel. Thus, viral ribonucleoproteins (vRNP) dissociate from M1 matrix protein. The released vRNP, which possesses nuclear localization sequences, enters the nucleus accordingly. Once inside the nucleus, viral polymerase starts the synthesis of viral mRNA which in turn being transported to the cytoplasm for further translation process to become viral proteins. These viral surface proteins, i.e. HA, NA and M2 ion channel, are processed in the host's endoplasmic reticulum, then glycosylated in Golgi apparatus before they are transported to the cell membrane. As for vRNPs, its complex with M1-NS2 proteins interacts with human chromosome region maintenance 1 (CRM1) protein which enable them to be exported from the nucleus to the cytoplasm and finally reaching the cell membrane to be incorporated into new virus that is budding out. HA and NA of new viruses contain terminal sialic acid that hold the viruses on the cell surface. At the last stage, NA of the new viruses cleaves these sialic acid residues, helping the virus to be released from the host cell and spread to continue its infectious action to the other cells (Das et al., 2010).

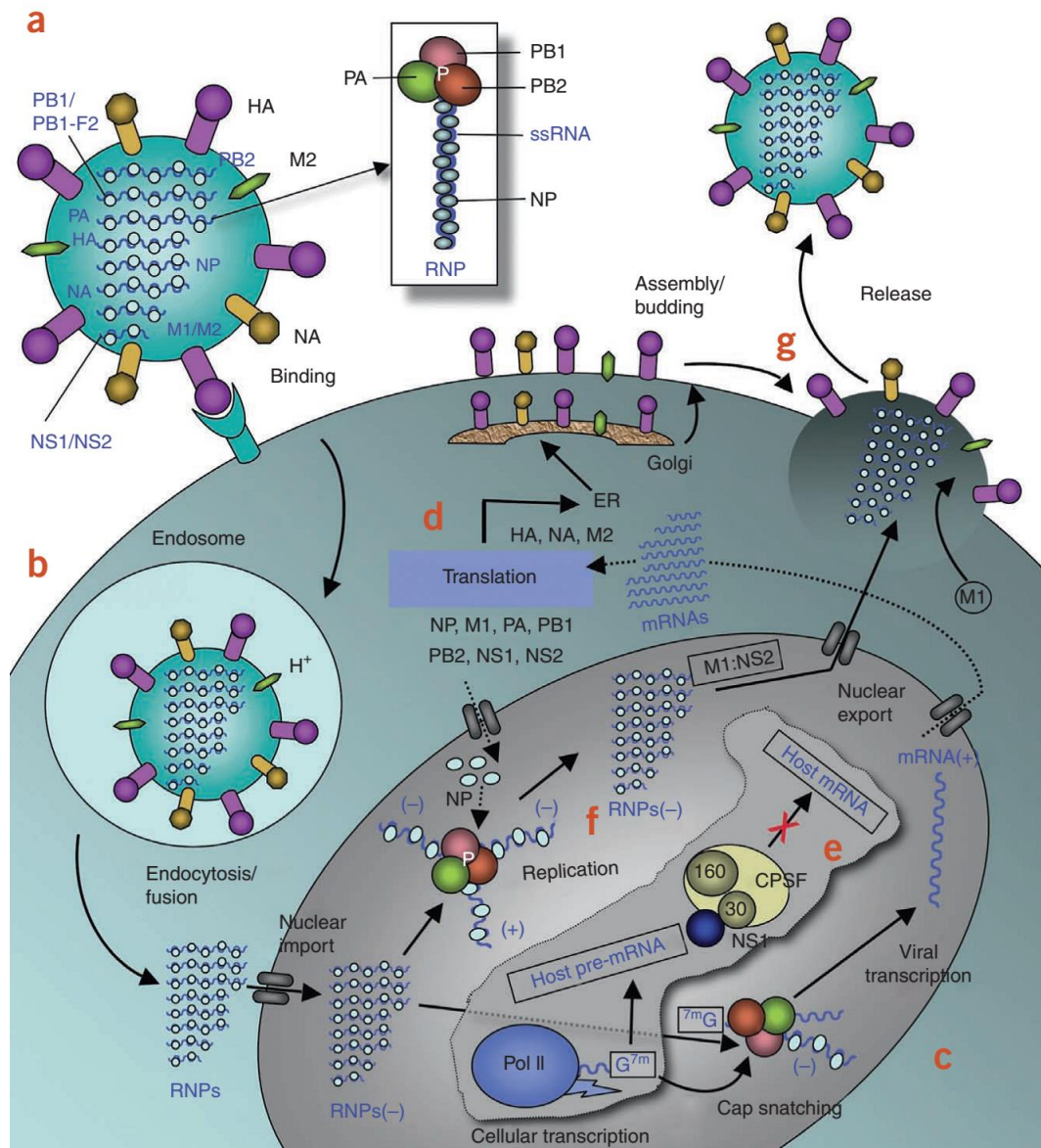


Figure 2.2. Life cycle of influenza A virus (Das et al., 2010).

It has been evidenced that influenza virus evolved through antigenic shift and antigenic drift. The latest pandemic H1N1 2009 strain is known to be derived from Eurasian swine H1N1 and North American swine H1N1, which are descendants of avian influenza gene pool and 1918 human H1N1, respectively. As mentioned above, avian influenza and human influenza viruses have distinct characters when transmitted into human. The first one is mostly high pathogenic but slowly spread among human,

while the latter has lower pathogenicity but easily spread among human. Therefore, one of the worst scenario in the evolution of influenza virus is the combination of two dangerous features: highly pathogenic and highly transmissible to human (Morens et al., 2009). For this reason, it is not an exaggeration to say that human influenza pandemics are unavoidable, but the extent of victims' number affected is unpredictable.

In the evolution of influenza virus, genetic changes have occurred since the influenza pandemic in 1918, either through antigenic shift or antigenic drift. Antigenic shift occurred when a strain of virus is able to jump from one species to another, e.g. avian to human. There are three different schemes of antigenic shift: (1) genetic mixing of human influenza and bird influenza in an intermediate host cell (swine) as mixing vessel, (2) the ability of avian influenza strain to directly jump into human without genetic change, and (3) the ability of avian influenza strain to enter an intermediate host (swine) and then to human without genetic changes (see Figure 2.3).

As opposed to antigenic shift, antigenic drift is a natural mutation in a strain of influenza virus which enable the virus to escape from the present antibody. For example, genes of HA in influenza virus have undergone some mutations which consequently changed the structural shape of HA. Thus, antibody which previously binds to HA loss its complementarity with HA and allows the newly mutated influenza virus to infect host cell (see Figure 2.4).

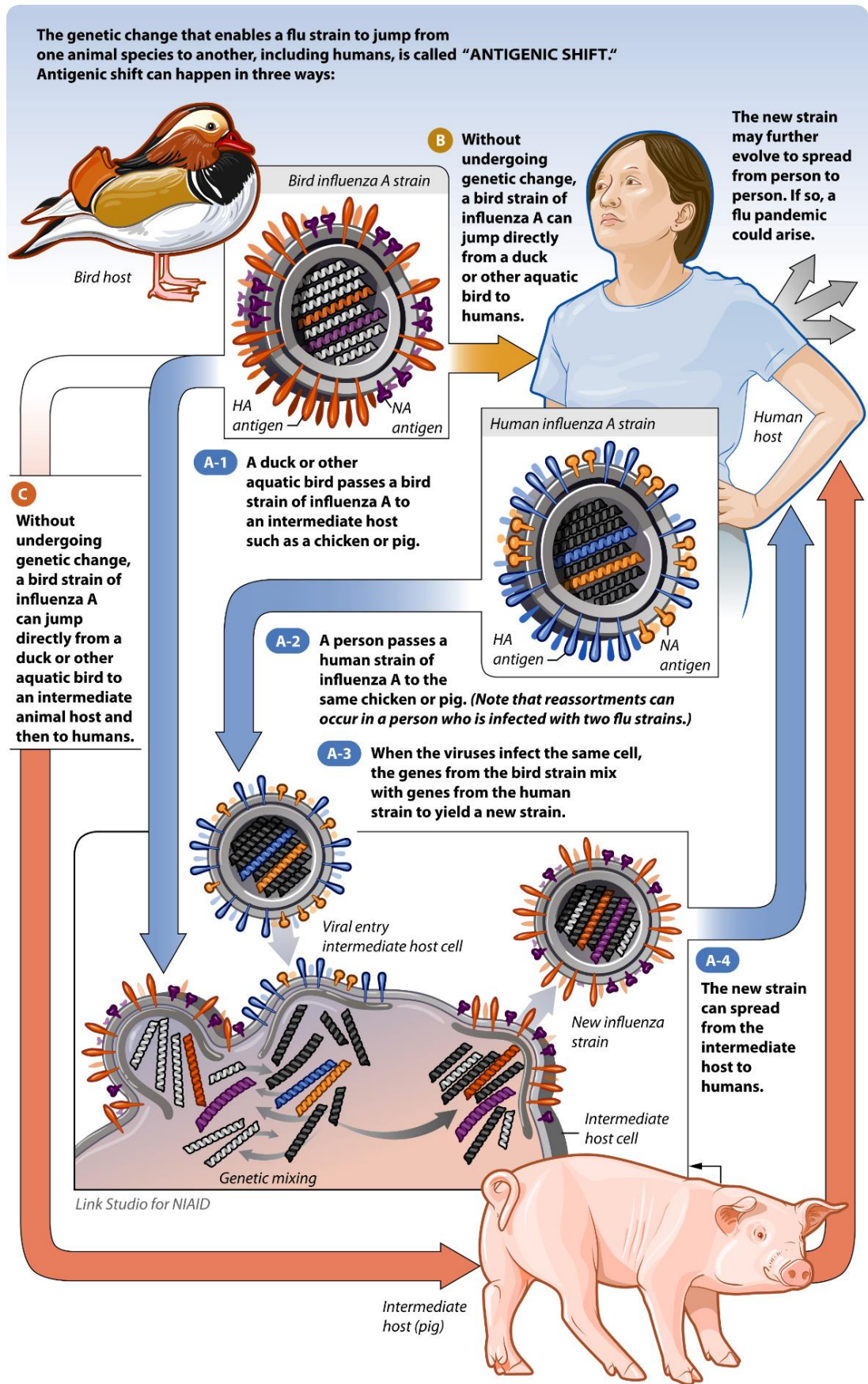


Figure 2.3. Antigenic shift in influenza virus. (US National Institute of Allergy and Infectious Diseases (NIAID)).

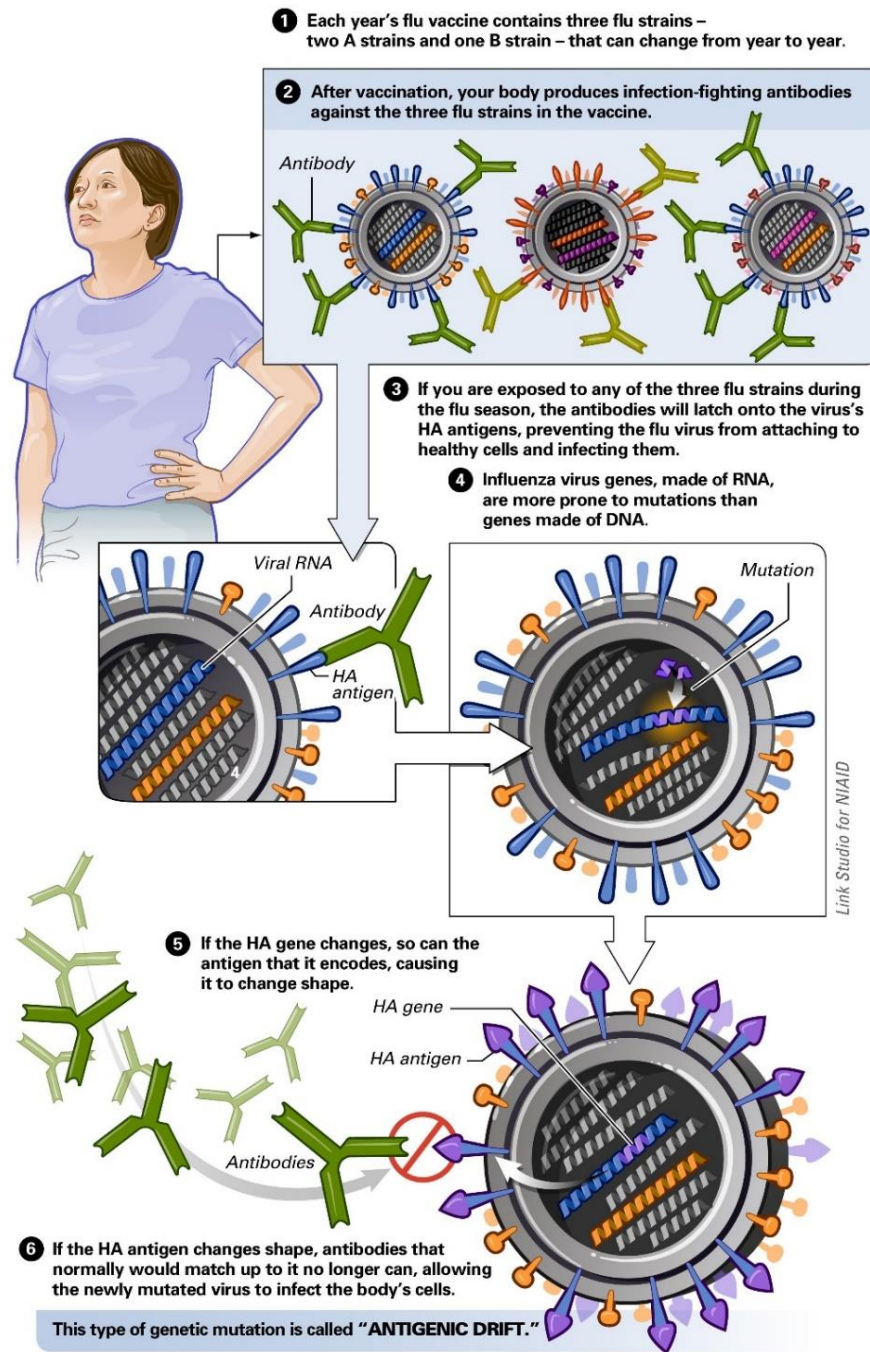


Figure 2.4. Antigenic drift in influenza virus (US National Institute of Allergy and Infectious Diseases (NIAID)).

Antigenic shift and drift in influenza virus have been proven as sources of repeating pandemics and endemics of influenza. The latest pandemic influenza in 2009, known to be caused by H1N1, was found as the results of gene re-assortments of swine influenza virus which is also another genetic product of the remarkable 1918 virus (Morens et al., 2009).

“Luckily”, the influenza virus appeared to evolve towards optimal transmissibility rather than pathogenicity. This is reflected from the decreased severity caused by influenza pandemics over time, although the advances in medicine and public health have also contributed. It is appeared that those highly pathogenic strains of influenza virus, e.g. H5N1 and H7N9, are not optimally transmissible. Nevertheless, there is still a possibility of entirely new virus which possesses the two most dangerous features, i.e. highly transmissible and pathogenic in human. (Morens et al., 2009). One of recent products of the evolution of influenza virus is avian influenza H7N9, which was found in 132 patients and resulted in 37 deaths in China (as of May 30, 2013). This new virus is different from other H7N9 viruses previously found in birds and for the first time in history has been shown to infect human (CDC, 2013).

Major efforts in preventing and controlling the influenza virus are through the development of vaccine and antiviral agents (Stiver, 2003). However, the current in-market vaccine is still susceptible to the antigenic evolution occurred in influenza virus (Gerhard W, 2006), thus it needs to be annually reformulated to cope with its limited protection in cases of antigenic mismatch (Pica and Palese, 2013). For this reason, antiviral agent can act as a first line of defence against the spread of influenza while providing some time for the completion of effective vaccine development in human pandemic setting. Currently, the largest stockpile of anti-influenza is oseltamivir (OTV), branded as Tamiflu, a NA inhibitor. NA is one of the most targeted proteins in drug discovery for influenza, mainly due to its conserved nature and important role in virus infection. Unfortunately, influenza virus can also build resistance towards NA inhibitors, thus the continuous efforts in antiviral development become very important (Itzstein and Thomson, 2009). Some of important mutations related to OTV-resistances in NA are H274Y, R292K and N294S. Among these three mutations,

H274Y has been a major concern in N1 subtype of NA due to its high resistance on OTV, without affecting the viability of influenza virus. Interestingly, H274Y has caused NA to become resistant to OTV, but not to zanamivir (ZMR), another licensed drug for influenza, branded as Relenza. Despite its high affinity on H274Y mutant, ZMR is known for its polarity problem and poor bioavailability. Although N2 subtype with H274Y does not naturally exist, studies have shown that H274Y-recombinant of N2 subtype is still sensitive to OTV (Abed et al., 2006; Wang et al., 2002).

It is reported that the pathogenicity of H5N1 strains was not affected by N294S mutation (Hay et al., 2008). Whilst, R292K mutation has resulted in poor viability and transmissibility of the virus despite its high level resistance on OTV (Carr et al., 2002; Herlocher et al., 2002). Recent H7N9 outbreak has also been reported to complicate OTV resistances caused by R292K mutation (Hu et al., 2013).

2.1.1. Neuraminidase (NA)

NA is a homotetrameric protein, in which, each monomer consists of six topologically identical four stranded antiparallel β -sheets and arranged like a propeller blades (Varghese et al., 1983). NA is an enzyme which cleaves the α -2,3 and α -2,6 glycosidic bond between terminal sialic acid (neuraminic acid, NANA) and galactose. The active site of NA (Figure 2.6) is composed of ten polar residues (e.g. arginine, aspartic acid, and glutamic acid) and four hydrophobic residues (e.g. alanine, isoleucine, and tryptophan) (Stoll et al., 2003). The active site of NA is conserved, hence NA is a favorable targeted protein for inhibitors in anti-influenza drug design, in addition to the availability of NA crystal structures in Protein Data Bank (Itzstein and Thomson, 2009).

The substrate-binding site (the top region of NA), is made up of loops, namely 150-, 200-, 220-, 250-, 270-, 300-, 320-, 330-, 340-, 370-, 400-, and 430- loops (see Figure 2.6a). The important role of 150-loop in inhibitor binding has been reported (Wu et al., 2013). While loops containing residues H274 and N294 (270- and 300-loops, respectively) were suggested as negatively-charged binding funnel of NA (Le et al., 2010). H274, R292 and N294 are points of mutation usually observed in NA. H274 is located at 270-loop while R292 and N294 are located at 300-loop. Amongst these three mutations, only R292 directly interacts with the ligand. Whilst H274 and N294 were regarded as two of the framework residues to support the structure of the catalytic site (Gubareva et al., 1997; Klenk et al., 2008). Although H274 and N294 do not directly interact with the ligand, it is expected that the mutations of H274Y and N294S would affect the conformation of surrounding loops, altering the integrity of NA's active site and the interaction of OTV-NA. There are two major groups of NA, i.e. Group-1 (N1, N4, N5 and N8 subtypes) and Group-2 (N2, N3, N6, N7 and N9) of NA, respectively (Collins et al., 2008). Besides N1-subtype (e.g. H1N1 and H5N1 viruses), N2-subtype also contributed to the major pandemics, i.e. H2N2 (Asian Flu) and H3N2 (Hongkong Flu) (Cox and Subbarao, 2000). In addition to H1N1, the H3N2 virus is also a major cause of severe epidemics. Therefore the understanding of N2-subtype in drug resistant case is critical for the preparedness against highly transmissible virus (Wu et al., 2013). The overlaid structures of N1 (PDB 2HU4 (Russell et al., 2006)) and N2 (PDB 1NN2 (Varghese and Colman, 1991)), showed that the active site residues in N1- and N2- are mostly conserved, except residues 246 and 347 (serine and tyrosine in N1 while alanine and glutamine in N2) (Figure 2.6b). For this reason, the difference of resistance level of H274Y mutant of N1- and N2-subtypes towards OTV (Wang et al., 2002), is also interesting to be studied.

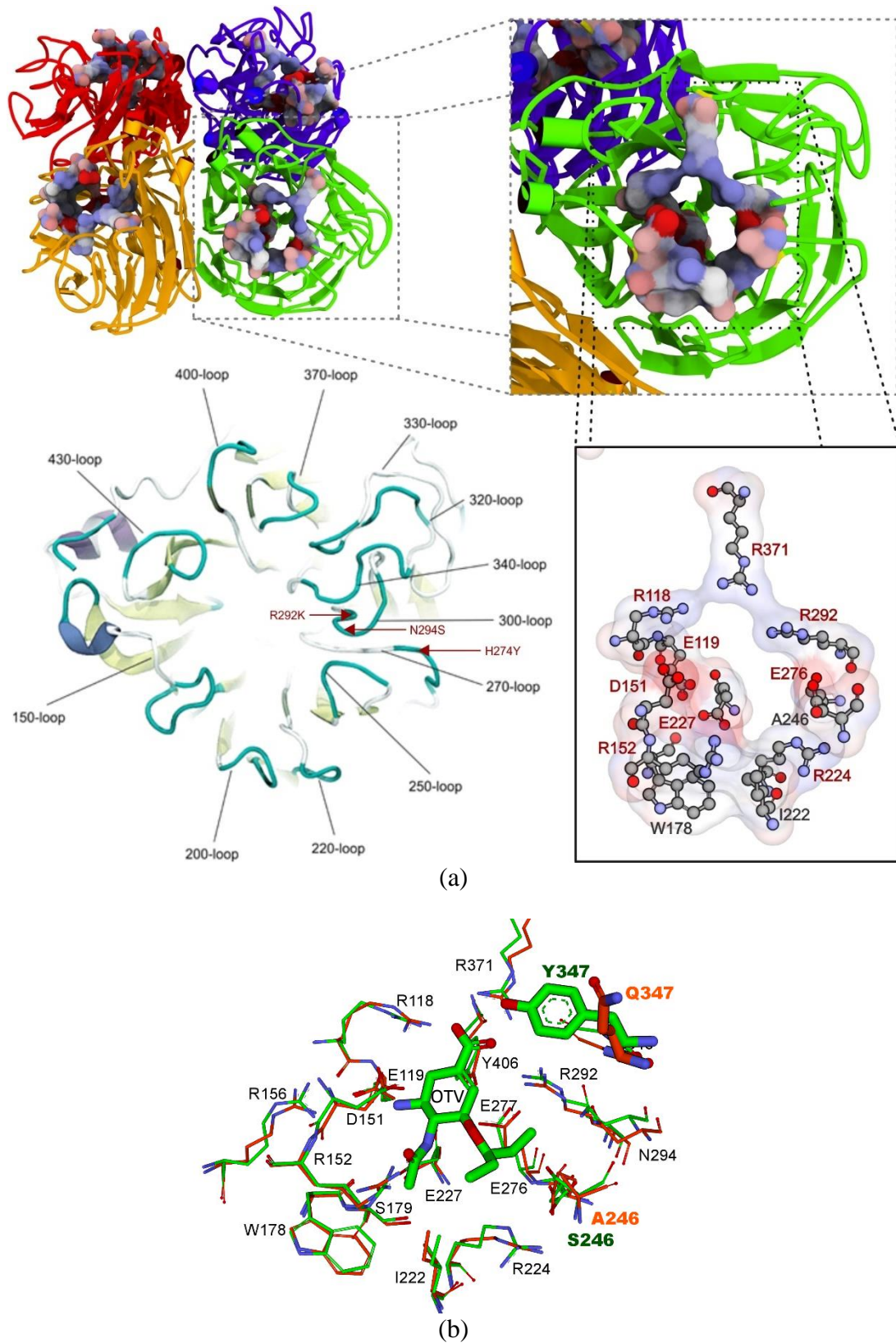


Figure 2.6. (a) Homotetramer NA which binding site located on top region. NA binding site composed mostly by polar residues (adapted from Stoll et al., 2003). (b) Residues within 5 Å from OTV in N1- and N2- subtypes (colored in green and orange, respectively). The figure was generated using Accelrys Visualizer and VMD.

2.2. The Development of Neuraminidase Inhibitors

The first NA inhibitor, 2-deoxy-2,3-didehydro-N-acetylneuraminic acid (DANA) which is a transition state analogue of NANA (NA substrate), was first reported by Meindl et al. (1974). Since then, DANA has served as a lead compound for the current FDA-approved neuraminidase inhibitors: Relenza (zanamivir) (von Itzstein et al., 1993) and Tamiflu (oseltamivir phosphate) (Kim et al., 1997) (reviewed in De Clercq, 2006).

Based on the crystal structure of NA (N2-subtype), von Itzstein and colleagues found that the binding pocket for C4 position of DANA may accommodate the larger basic group. Further investigation has led them to introduce guanidino moiety to fill up this site, which proven later to significantly interacted with E119 and E227, displaced a water molecule at C4 binding site, thus possessed a slow binding properties. This modified compound, zanamivir (ZMR), showed sub-nanomolar inhibition against influenza A (N2-subtype). Unfortunately, ZMR has poor oral absorption due to its polar nature. Therefore, ZMR is only delivered through inhalation to reach the primary target of infection (reviewed in Itzstein and Thomson, 2009).

The structural information derived from NA in complex with ZMR, DANA, and other related compounds have again been found useful in designing other potent inhibitors. It was found that the oxygen atom at dihydropyran ring on these compounds (e.g. ZMR, DANA) does not form important interaction with the active site (Taylor and von Itzstein, 1994), which indicated the possibility to replace this oxygen atom with carbon atom. Consequently, Kim and colleagues developed a new NA inhibitor based on carbocyclic, cyclohexene-based which was derived from shikimic acid (Kim

et al., 1997). They observed that the hydrophobic backbone of glycerol moiety in DANA and ZMR interacted with NA active site, thus suggested the possibility to replace the whole glycerol side chain with hydrophobic alkyl group in order to improve the oral bioavailability of the compound. Finally, an optimized structure resulted from further structure-activity relationship (SAR) studies, i.e. oseltamivir carboxylate (OTV) is produced and now marketed as Tamiflu (prodrug of OTV). As compared to DANA, OTV has pentyloxy group at position C6 (as replacement of glycerol moiety in DANA and ZMR), and an amino group at position C4 (Figure 2.7). Moreover, OTV also possessed a slow binding characteristic due to the requirement of hydrophobic sub-pocket formation by E276 and R224 during its binding (Kati et al., 1998; Itzstein and Thomson, 2009).

After the discovery of OTV, the overlaid crystal structures of a furanose isomer with DANA in complex with N9 subtype has revealed that the four functional groups (side chains) in both complexes had similar orientation and interactions in the binding site. Therefore, it was concluded that the central ring is not an absolute factor in the development of potential NA inhibitors. Instead, it is the relative position of the functional groups in the active site which is important (Babu et al., 2000). For this reason, cyclopentane-based compounds (different central ring from the previous compounds) were developed and as a result peramivir (PMV) was discovered. PMV possesses a branched 2'-ethylbutyl side chain (analogue with OTV's pentyloxy) which is expected to have similar features with OTV in optimal interaction with the hydrophobic sub-pocket in NA active site. As for C4 position, PMV has a guanidino moiety similar to ZMR. In 2006, FDA approved the usage of PMV in injectable formulation (reviewed in Itzstein and Thomson, 2009).

In 2009, Yamashita and colleagues (Yamashita et al., 2009) reported the new potent NA inhibitors, i.e. laninamivir (LNV) and its prodrug: laninamivir octanoate. LNV possesses a guanidino group at position C4 and polyhydroxy group at position C6, similar to ZMR. However, at position C6, one of hydroxyl at 1'-glycerol was replaced with methoxy group. Moreover, LNV was found to be active against N1-N9 subtypes, including OTV resistant strain, i.e. H274Y mutant. In addition, it is reported that its prodrug was shown to have long-acting properties as NA inhibitor. LNV showed a good efficacy in mouse model despite being administered 7 days before influenza infection (Yamashita, 2010), whereas Relenza and Tamiflu required twice-daily administrations for the treatment. The long-acting properties of LNV prodrug was predicted due to its long retention in the lung. However, further clinical study (Watanabe et al., 2010) has shown that LNV prodrug was not significantly better than OTV in treating H274Y H1N1 in adult patients. It is suggested that in adult patients, LNV octanoate was slowly processed into its active form (Vavricka et al., 2011). Nevertheless, in 2010, LNV has been approved for anti-influenza drug in Japan and marketed under name of Inavir. The chemical structure of compounds reviewed above, are presented in Figure 2.7.

Further development of NA inhibitors, based on OTV structure, were performed by Xie et al. (2014) and Mooney et al. (2014). The new structures were designed by extending the amino group of OTV (at C4 position) to target the 150-cavity of NA. Two derivatives showed better potency against H5N1 NA than OTV (Xie et al., 2014). In another study, introducing the guanidine group to substitute the amino group of OTV also improve the ligand binding with NA of H1N1 and H5N1 (Mooney et al., 2014).

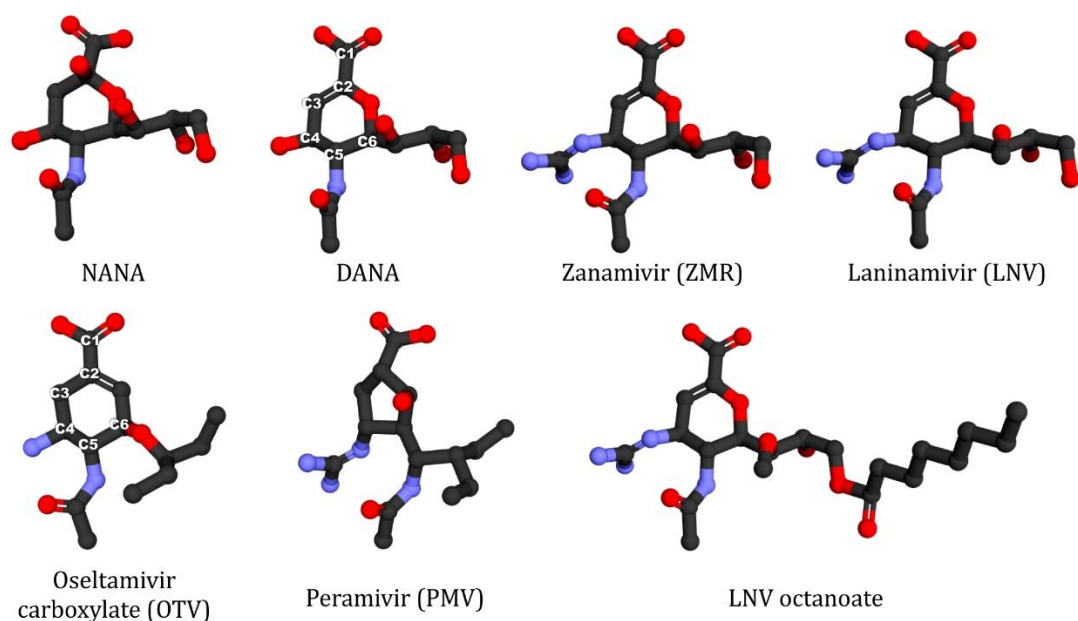


Figure 2.7. Three dimension chemical structures of NANA (substrate), DANA, ZMR, OTV, PMV, LNV and LNV octanoate. The figure was generated using Accelrys Visualizer.

2.3. Resistance to Neuraminidase Inhibitors

Since Tamiflu is the world's largest stockpile of anti-influenza drug, the increased report of OTV resistant strains has raised some awareness (Hayden, 2006; Moscona, 2005; Soundararajan et al., 2009; Hurt et al., 2009; Liu et al., 2013; Abed et al., 2006; Stephenson et al., 2009). Most recently, in 2015, Gillman and colleagues suggested that exposure of OTV to the aquatic environment might contribute to the evolution of avian influenza virus strain that are potentially pathogenic to human (Gillman et al., 2015). For these reasons, the careful use of OTV is critical to limit the development of mutant virus. Therefore, deep understanding on the mechanism of OTV resistances, especially at the molecular/atomic level, has become very important.

Figure 2.8 presents the overview of many studies which conducted in an attempt to uncover the mechanism of OTV resistances due to H274Y mutation (Wang et al., 2002; Collins et al., 2008; Park and Jo, 2009; Malaisree et al., 2009; Wang and Zheng, 2009; Le et al., 2010; Rungrotmongkol et al., 2010; Karthick et al., 2012). In a mutagenesis study (Wang et al., 2002), it was observed that residues with bulkier side chain (i.e. tyrosine, phenylalanine) reduced the NA sensitivity towards OTV, by posing steric hindrance for reorientation of the nearby E276. The rearrangement of E276 was required to form a proper hydrophobic pocket for OTV (Itzstein and Thomson, 2009; Kati et al., 1998). This effect, however, was not observed when involved smaller residues or ligands with glycerol moieties attached to them, such as zanamivir (ZMR) and 4-amino-DANA (See Table 2.1). Interestingly, OTV affinities in H274Y mutant of recombinant H3N2 was not affected (Wang et al., 2002), suggesting that the differences in residues surrounding position 274 in N2 and N1 subtypes, play an important role in contributing the resistance to OTV.

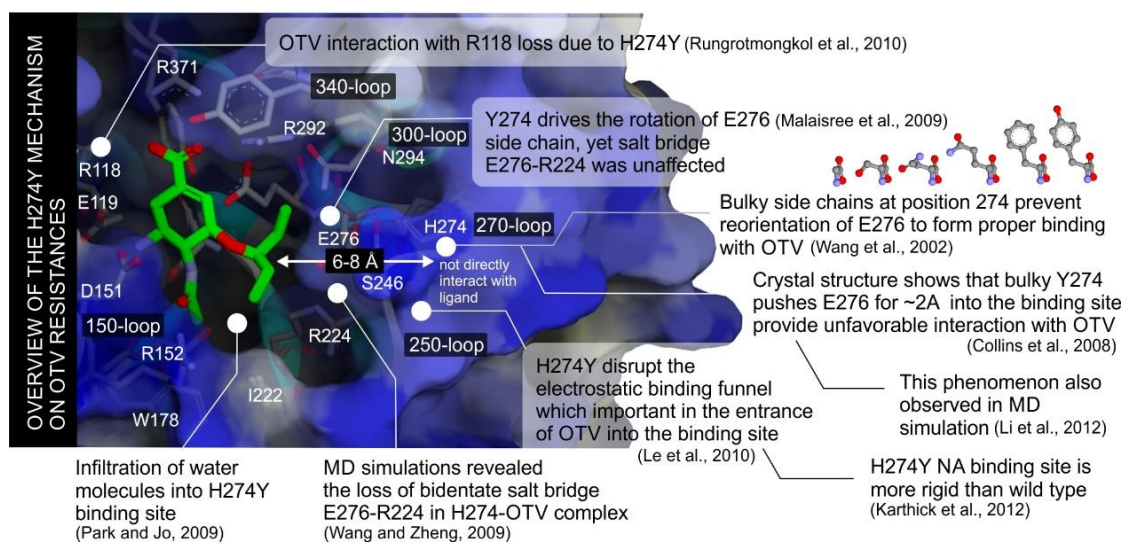


Figure 2.8. Binding mode interaction of OTV (green colored sticks) in NA's active site and the overview of hypotheses on H274Y effects towards the mechanism of OTV resistance. The figure was generated using Accelrys Visualizer.

Table 2.1. The effect of different size of amino acid's side chain at the position of 274 towards K_m values of 2'-(4-Methylumbelliferyl)- α -D-N-acetylneuraminic acid (MUNANA) and K_i values of OTV, ZMR, and 4-amino-DANA (adapted from Wang et al., 2002).

Type of recombinant NA (A/WS/33 H1N1)	K_m (μ M) of MUNANA	K_i (nM)		
		OTV	ZMR	4-amino-DANA
Wild type (H274)	31	0.3	0.1	50
H274G	100	0.2	5.7	1140
H274S	110	0.1	14.9	890
H274N	133	0.1	6.0	1250
H274Q	125	0.5	3.8	940
H274F	57	86.0	0.4	130
H274Y	55	105.0	0.3	150

The results obtained from the mutagenesis study (Wang et al., 2002) was supported by the NA crystal structures of H274Y mutant (from H5N1 virus) in complex with OTV and ZMR (Collins et al., 2008). As observed in the crystal structure of H274Y-OTV complex (PDB ID: 3CL0), Y274's bulky side chain pushes E276's carboxylate side chain ~ 2 Å deeper into the binding site (compared to that in the wild type). This resulted in the disruption of hydrophobic pocket which could no longer accommodate OTV's pentyloxy group. However, the disruption did not affect the two hydroxyl groups of ZMR to maintain the interaction with the carboxylate group of E276 (Figure 2.9).

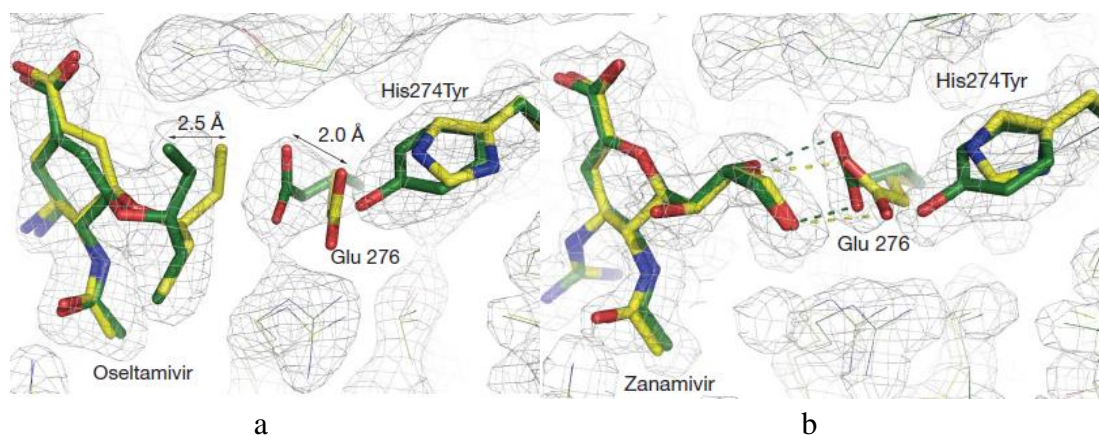


Figure 2.9. (a) The molecular basis of N1 resistance towards OTV derived from H274Y crystal structure (PDB ID 3CL0, green colored carbon atoms) which overlaid with wild type (yellow colored carbon atoms). (b) The overlaid of H274Y-ZMR complex (PDB ID 3CKZ, green colored carbon atoms) with wild type (Collins et al., 2008).

This observation was in agreement with the molecular dynamics (MD) studies on H274Y-OTV complex system, where the conformational change of E276 (Li et al., 2012; Wang and Zheng, 2009) and the loss of bidentate salt bridge between E276 and R224 (Wang and Zheng, 2009) were also observed. The MD results showed that Y274 forced the rotation of E276's carboxylate group's side chain by 115° thus altered the hydrophobic sub-pocket. Due to the altered binding site, the pentyloxy group of OTV was rotated by 125° , thus reducing the binding energy by ~ 5 kcal/mol (Malaisree et al., 2009) (Figure 2.10).

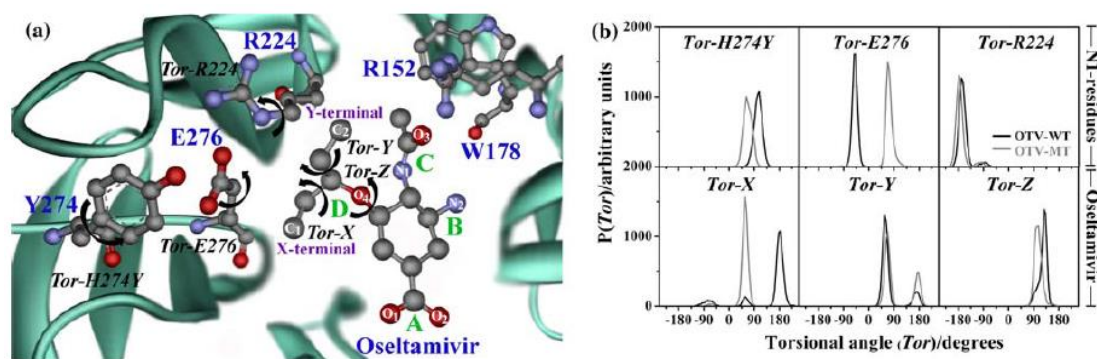


Figure 2.10. Rotational changes of binding residues (Y274, E276 and R224) and pentyloxy group of OTV (Tor-X, Tor-Y and Tor Z) which represented in (a) molecular diagram and (b) plot of dihedral angle distribution (taken from Malaisree et al., 2009).

In another MD simulation study of OTV-H274Y complex system, it has been proposed that the origin of OTV resistance was due to the infiltration of water molecules into the binding site (Park and Jo, 2009) (Figure 2.11). MD studies of various mutants (e.g. H274Y, N294S and R292K) in complex with OTV (Rungrotmongkol et al., 2010; Ripoll et al., 2012) indicated that each mutation has resulted in different conformational changes at the active site. Therefore, the mechanism of drug resistances in various mutants should not be generalized (Figure 2.12). Furthermore, the differences between the buried surface areas of OTV's pentyloxy in the WT and in H274Y (Table 2.2), were not in agreement with those suggested from the crystallography data (Collins et al., 2008).